Hydrophobic lithiated titania floating film for efficient solar-driven water evaporation

Miaomiao Ye, Xun Wang, Pei Zhou, Rong Chen, Qimao Gan and Tuqiao Zhang

ABSTRACT

Recently, the development of new photothermal materials for seawater desalination based on air–water interfacial solar heating has become a new research hotspot. In this paper, hydrophobic lithiated titania was synthesized by lithium reaction with amorphous titania followed by surface modification with a thin 1H,1H,2H,2H-perfluorooctyltrichlorosilane (PFOTS) monolayer. The hydrophobic lithiated titania was used as a photothermal material for seawater evaporation based on this new process. A thin lithiated titania floating film was assembled under simulated solar light irradiance due to the combined actions of water surface tension and the water molecules' thermal motion. The formation of the thin floating film significantly promoted water evaporation. The water evaporation rate by the lithiated titania floating film was 0.87 $kg{\cdot}m^{-2}{\cdot}h^{-1}$ under 2.0 sun solar irradiance, which was 2.4 times higher than that of pure water. Parameters affecting the solar evaporation process such as lithiated titania dose, solar light intensity, and storage time were investigated. Finally, the quality of the condensed fresh water was tested to evaluate the potential application of the lithiated titania floating film in practical settings of seawater desalinization.

Key words | floating thin film, hydrophobic lithiated titania, interfacial solar heating, water evaporation

Miaomiao Ye
Xun Wang
Pei Zhou
Rong Chen
Qimao Gan
Tuqiao Zhang (corresponding author)
Zhejiang Key Laboratory of Drinking Water Safety and Distribution Technology, College of Civil Engineering and Architecture,
Zhejiang University,
Hangzhou 310058,
China
E-mail: *ztq@zju.edu.cn*

INTRODUCTION

Recently, seawater desalination based on air–water interfacial solar heating has attracted increasing attention due to its high water evaporation rate, the high quality of the condensed fresh water, simple operation, low energy consumption, low cost, etc. (Wang *et al.* 2018; Zhu *et al.* 2018a). This new desalination technology has been labeled as a reliable method to solve the water shortage problems in some remote and rural areas where electric power and centralized water desalination are still unavailable (Chandrashekara & Yadav 2017; Chen *et al.* 2017b). Photothermal materials, which float on the water surface and only heat the air–water interface while avoiding uniformly heating the bulk water, are considered as the most important link in this new desalination process. Up to now, four types of photothermal materials including (1) carbon-based materials (Dao & Choi 2018; Gan *et al.* 2019), (2) plasmonic metal nanoparticles (Hu *et al.* 2016; Zhou *et al.* 2016), (3) metallic oxides (Chen *et al.* 2017a; Wang *et al.* 2017), and (4) some unique materials (Xu *et al.* 2017; Chen *et al.* 2019) have been synthesized and employed for seawater desalination based on the above new process. Among them, metallic oxides are relatively less studied as metallic oxides with wide absorption capability covering the full solar spectrum are rare. However, metallic oxides have advantages over other photothermal materials as they have good chemical stability, excellent mechanical strength, are non-toxic and have low cost. Some magnetic metallic oxides can be easily separated from solution therefore

doi: 10.2166/ws.2019.179

avoiding the contamination of the seawater. To float on the water surface, photothermal materials are usually immobilized on floating supports such as air-laid paper, mesh, cellulose membrane, sponge, foam etc. to form solar stills (Ding *et al.* 2017; Liu *et al.* 2017; Tao *et al.* 2018). The deposition on supports will lead to the inadequate utilization of these photothermal materials since part of the material surfaces adhere to the supports. In some cases, they may detach from the support since the immobilization is typically realized through physical adhesion (Liu *et al.* 2015; Wang *et al.* 2016). In addition, salt accumulation will happen in some solar stills under continuous operation, resulting in lowered water evaporation rates and destroyed solar stills (Shi *et al.* 2018; Zhu *et al.* 2018b).

In this paper, hydrophobic lithiated titania was synthesized by lithium reduction with amorphous white TiO_2 nanoparticles followed by deposition of a monolayer of 1H,1H,2H,2H-perfluorooctyltrichlorosilane (PFOTS) on their surfaces. A very small amount of lithiated titania was used as the photothermal material for water evaporation based on interfacial solar heating. A thin lithiated titania film self-assembled under simulated solar light irradiance with the assistance of the water's surface tension and water molecules' thermal motion. The as-formed thin floating film could achieve close contact with the water surface to ensure efficient heat transfer so that the water evaporation rate could be significantly enhanced. The salt-rejecting property of the thin floating film was also achieved through the hydrophobic surface of the materials. The main purposes of this study are: (i) to obtain hydrophobic lithiated titania for solar evaporation; and (ii) to check the effect of formation of a thin film on the water evaporation rate and the salt-rejecting property.

MATERIALS AND METHODS

Preparation of hydrophobic lithiated titania

The preparation of hydrophobic lithiated titania was divided into the following three steps. (1) Synthesis of white amorphous TiO_2 (Ye *et al.* 2010): 100 mg of hydroxypropyl cellulose (HPC, $M_w = 80{,}000$) was mixed with 0.12 mL of distilled water and 25 mL of absolute ethanol under vigorous magnetic stirring. A tetrabutyl titanate (TBOT) solution (1 mL TOBT dissolved in 5 mL of ethanol) was introduced drop by drop, followed by refluxing at 85 °C for 90 min. The white precipitates were collected by centrifugation and washed with ethanol several times, then dried at 60 °C for 4 h. (2) Synthesis of lithiated titania: 100 mg of the as-prepared white TiO_2 was mixed with 35 mg of lithium foil in a crucible, followed by heat treatment at a temperature of 250 °C for 12 hours under Ar atmosphere. The product was transferred to a quartz sand pond and exposed in air for 2 days, followed by washing with deionized water three times and drying in a vacuum. (3) Surface hydrophobization of lithiated titania: 300 mg of lithiated titania was transferred into 4 mL *n*-hexane containing 0.5% PFOTS, and the mixture was sonicated for 20 min and dried at 60 °C for 4 h to obtain the final product.

Formation of a thin floating film

The as-prepared hydrophobic lithiated titania powder was randomly dispersed on the surface of the water followed by irradiation under a 300 W CEL-S500 xenon lamp with intensity of 2,000 W/m^2 (2 sun) for 4 hours. A thin floating film was formed with the assistance of the water's surface tension and water molecules' thermal motion.

Water evaporation experiments

Water evaporation experiments were conducted at a temperature of 20±1 °C and air humidity of 45%±10%. Hydrophobic lithiated titania film was floated on the surface of 200 mL water in a 250 mL beaker. The beaker was placed on an electronic balance (FA2104, Shanghai Sunny Hengping Scientic Instrument Co., Ltd) to measure the unevaporated water. A 300 W CEL-S500 xenon lamp obtained from Beijing Zhong Jiao Jin Yuan Science and Technology Co, China, was used with an AM 1.5 filter to simulate solar light. The light source was vertically fixed to the water surface at a distance of 5 cm. The light intensity at the water surface was 2,000 W/m^2, as measured by a laser power meter (LP-3A, Beijing Physcience Opto-Electronics, China).

Characterization

The crystalline structure of the lithiated titania was characterized by X-ray diffraction (XRD) with Cu Kα radiation ($\lambda = 1.5406$ Å). The morphology of the lithiated titania and self-assembled film was analyzed using a transmission electron microscope (TEM, Phillips Tecnai 10) with an accelerating voltage of 100 kV and a scanning electron microscope (SEM, Hitachi S-4800) respectively. The ultraviolet–visible–near-infrared (UV–Vis–NIR) diffuse reflectance spectra of the lithiated titania was measured on a U-4100 UV–Vis–NIR spectrophotometer (Hitachi, Japan) equipped with an integrating sphere accessory. $BaSO_4$ powder was used as a 100% reflectance standard. The contact angle was measured by an OCA20 optical contact angle measuring device (Dataphysics, Germany). The temperature distribution of the floating solar still surface was measured by an S65 thermal infrared imager (FLIR, USA). The concentrations of anions and cations in the condensed fresh water were tested by a Dionex ICS-2000 ion chromatograph (Dionex, USA) and a PE NexION 300Q inductively coupled plasma mass spectrometer (Perkin Elmer, USA) respectively. The conductivity (salinity) was determined by an HQ14d conductivity meter (HACH, USA). The total organic carbon (TOC) was measured by a TOC-V_{CPH} TOC analyzer (Shimadzu, Japan). The turbidity was tested by a 2100Q01 portable turbidimeter (HACH, USA).

RESULTS AND DISCUSSION

Synthesis and characterization of hydrophobic lithiated titania

As shown in the inset of Figure 1(a), the white amorphous TiO_2 power obviously turned black after being reacted with lithium foil. The XRD pattern shows that the black powder was composed of Li_xTiO_2, Ti_xO_{2x-1} and Ti. Here, we

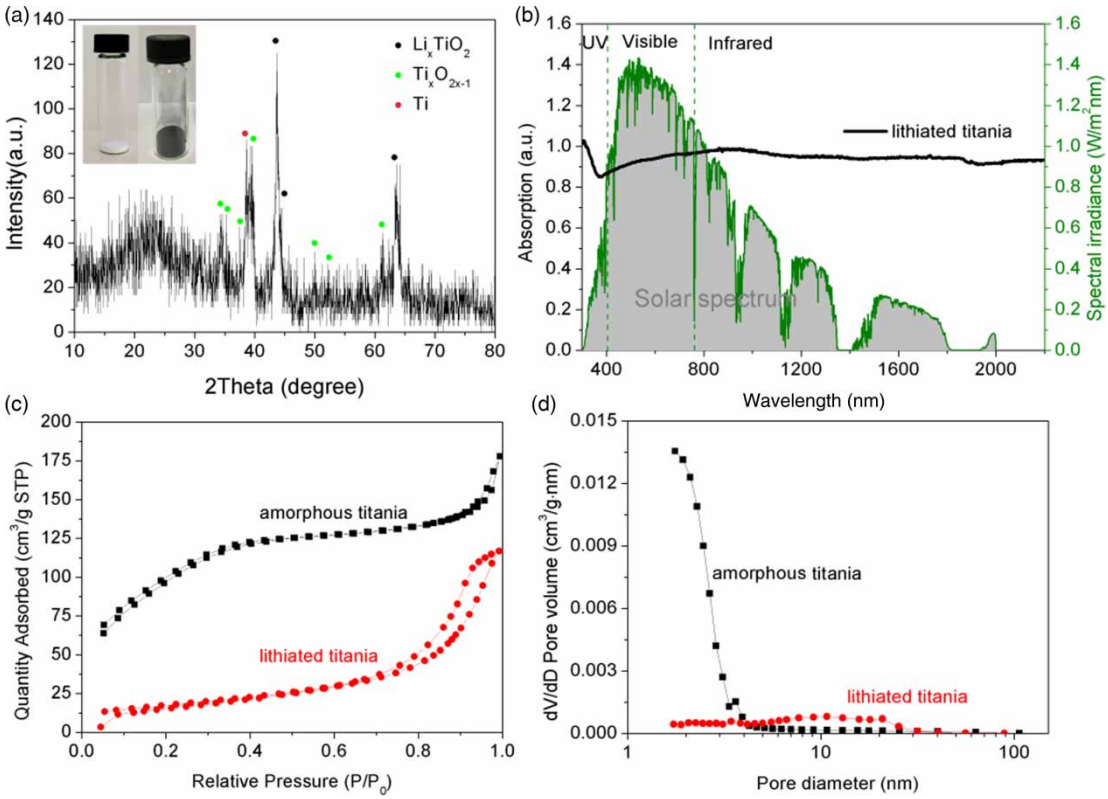

Figure 1 | (a) XRD pattern and (b) UV–Vis–NIR adsorption spectrum of lithiated titania; (c) N_2 adsorption–desorption isotherms and (d) BJH pore-size distribution curves of the amorphous and lithiated titania.

denote it as lithiated titania. Besides the color and crystalline phase change, the morphology and size of the TiO_2 was also dramatically destroyed during the lithium reduction process. Before lithium reduction, the amorphous TiO_2 was typically of spherical structure with an average external diameter of 0.79 μm (Figure S1a, Supplementary Material). The surface of the spheres was not smooth but was composed of numerous nanoparticles (Figure S1b). After lithium reduction, the spheres collapsed into numerous nanoparticles with an average size of 47 nm (Figure S1d).

The effects of lithium reduction on the porosities and surface areas of the lithiated titania were explored by measuring the N_2 adsorption–desorption isotherms, and the results are shown in Figure 1(c). Before lithium reduction, the isotherm was of the typical type I pattern without any hysteresis loops, indicating the existence of micropores according to the IUPAC classification (Sing *et al.* 1985). After lithium reduction, the isotherm converted to the typical type IV with distinct H4 hysteresis loop in the range of 0.6–1.0 P/P_0 appearing, which indicated the existence of mesopores (Sing *et al.* 1985). Compared with micropores, mesopores were beneficial to the enhancement of water evaporation since vapor could rapidly pass through. The corresponding pore-size distributions of the amorphous titania and lithiated titania were determined using the Barrett–Joyner–Halenda (BJH) method from the desorption branch of the isotherm (Figure 1(d)). The pore volumes of the amorphous titania and lithiated titania were 0.23 $cm^3 \cdot g^{-1}$ and 0.18 $cm^3 \cdot g^{-1}$, respectively. The slightly decreased pore volume was due to the crystallization of the titania during the lithium reduction calcination process.

Solar absorption ability is a very important property for a photothermal material. The absorption spectrum in the wavelength range from 200 to 2,200 nm of lithiated titania was measured via a UV–Vis–NIR spectrophotometer, and the result is shown in Figure 1(b). The proportion of solar absorption in different spectral regions from ultraviolet (<400 nm) to visible (400–760 nm) and near-infrared (760–2,200 nm) was calculated according to Equation (1) by using MATLAB software for the mathematical integral:

$$A = \frac{\int (1 - R) \cdot S \cdot d\lambda}{\int S \cdot d\lambda} \quad (1)$$

where A is the solar absorption, R represents the reflectance of the sample, λ represents the wavelength (nm), and S represents solar spectral irradiance ($W \cdot m^{-2} \cdot nm^{-1}$). As calculated, the total solar absorption of the lithiated titania was 88.57%, with ultraviolet light, visible and infrared light regions being 3.86%, 43.63%, and 41.08% respectively.

Formation of a lithiated titania floating film

The formation of a thin floating film on the water surface will enable more efficient use of the photothermal material for solar absorption. Here, the formation of a lithiated titania floating film can be realized by surface modification of the lithiated titania with a hydrophobic monolayer of PFOTS followed by solar irradiance. After PFOTS modification, the lithiated titania exhibited a hydrophobic surface with a contact angle of 137° (Figure 2(a)). The hydrophobic surface enabled the lithiated titania to be easily self-floated on the water surface (Figure 2(c)). After 4 hours solar irradiance with an intensity of 2.0 $kW \cdot m^{-2}$, a thin film self-assembled with the assistance of the water's surface tension and water molecules' thermal motion (Figure 2(d)). To further observe the morphology of the thin film, SEM analysis was carried out. Before observation, the self-assembled thin film was moved to a 1 cm × 1 cm commercial silicon wafer by the dip-coating method (Ye *et al.* 2012). As shown in Figure 2(b), a uniform film containing small clusters of the nanoparticles was observed. As the entire water surface was covered by the lithiated titania thin film, the solar absorption of the lithiated titania would be increased, therefore promoting water evaporation. It was also reasonable to think that the water evaporation rate could be optimized by tuning the thickness of the floating film.

Water evaporation

To check the advantage of the interfacial solar heating, a water evaporation experiment with the lithiated titania floating film was carried out. As a reference, water evaporation by itself and water evaporation by uniformly dispersed lithiated titania were also carried out. As shown in Figure 3(a), all of the water evaporation processes could be modeled by zero-order kinetics and simply described

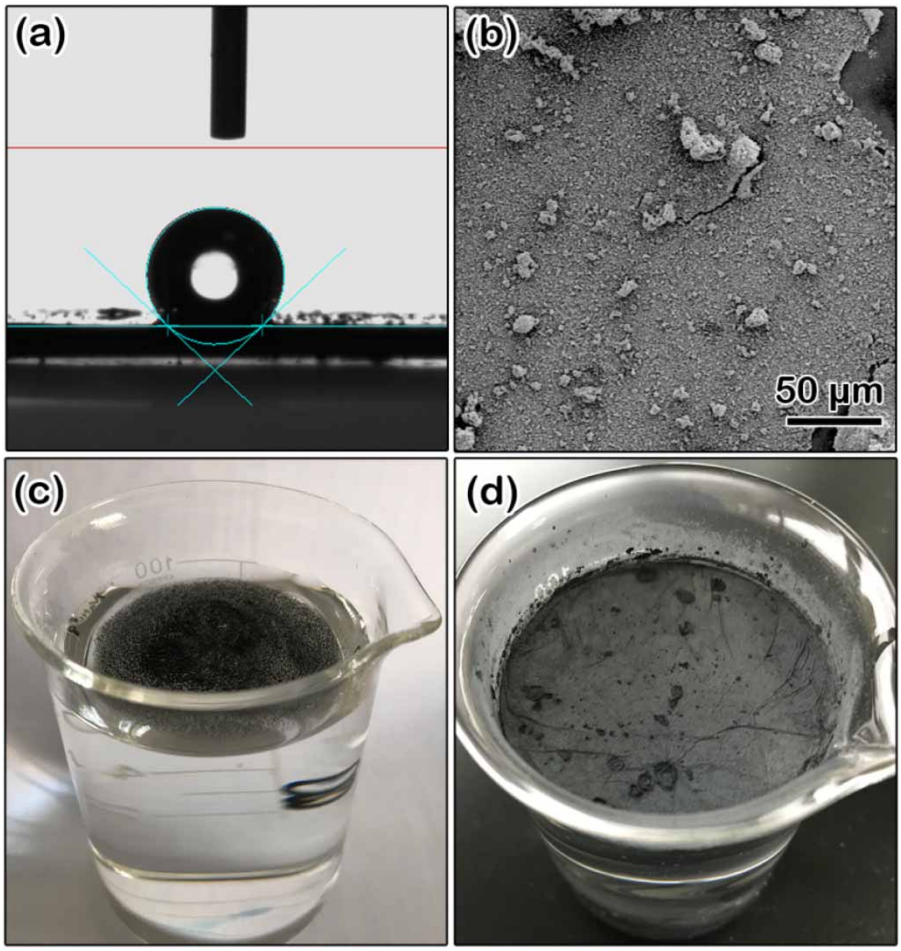

Figure 2 | (a) The contact angle of the hydrophobic lithiated titania, (b) the SEM image of the lithiated titania film, and digital photos of hydrophobic lithiated titania (c) before and (d) after formation of a thin floating film.

by Equation (2):

$$m - m_0 = kt \tag{2}$$

where m and m_0 are the actual water mass at time t and the initial water mass respectively, and k is the water evaporation rate. The zero-order kinetic equations and k values of the all water evaporation processes are presented in Table S1 (Supplementary Material). The k value of lithiated titania floating film was 0.87 $kg{\cdot}m^{-2}{\cdot}h^{-1}$ under 2.0 sun solar irradiance, which was 2.4 and 2.2 times higher than that of the control cases of pure water and water with uniformly dispersed lithiated titania, respectively. The significantly enhanced water evaporation rate of the lithiated titania film undoubtedly proved the advantage of the interfacial solar heating.

To further confirm the interfacial solar heating behavior, surface water temperatures during the solar evaporation process with and without lithiated titania film were monitored via the infrared thermal imager. Before solar irradiance, the surface water temperatures with and without lithiated titania film were 24.2 °C and 23.4 °C respectively (Figures S2 and S3, Supplementary Material). After 1 hour of 2.0 sun solar irradiance, the water surface temperature with lithiated titania film finally reached 49.2 °C, which was 11.5 °C higher than that without lithiated titania. The big temperature difference confirmed the interfacial heating behavior. The surface water temperatures versus time curves with and without lithiated titania were also recorded, and the result is shown in Figure 4. Compared with the black curve, the red curve quickly reached 39.6 °C in the first

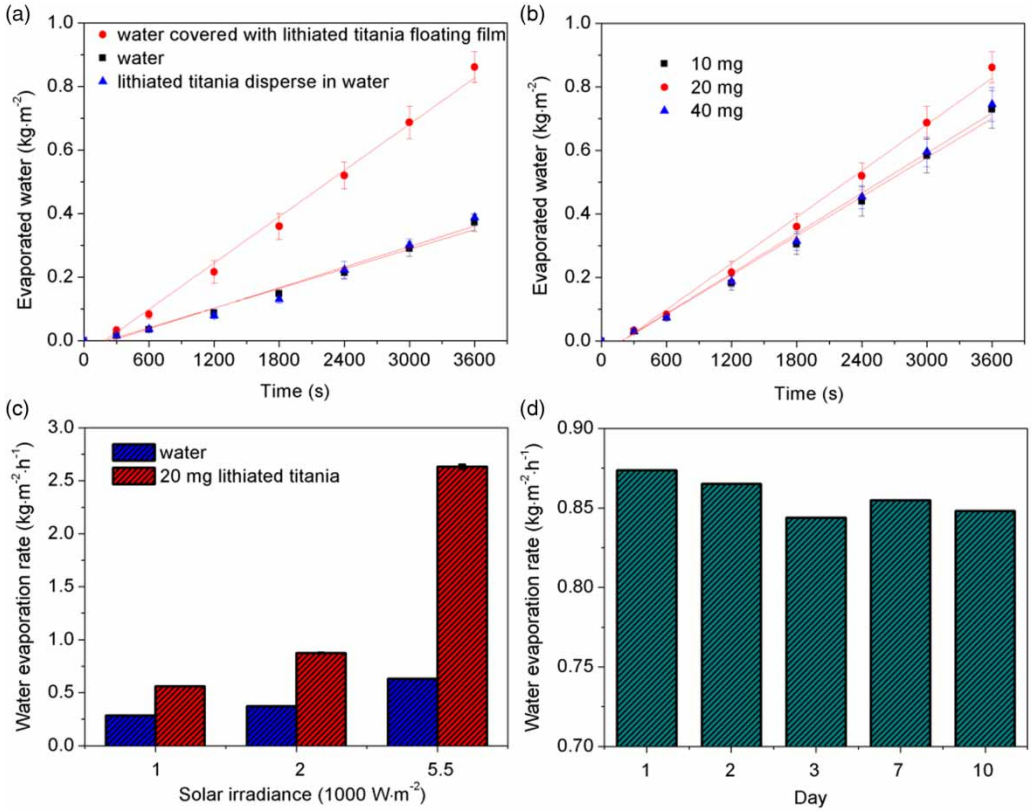

Figure 3 | (a) The mass of the evaporated water as a function of irradiance time in different evaporation processes; the effects of (b) lithiated titania doses and (c) solar light intensities on the water evaporation rate; (d) water evaporation rate of lithiated titania floating film under 2.0 sun solar irradiance within 10 days.

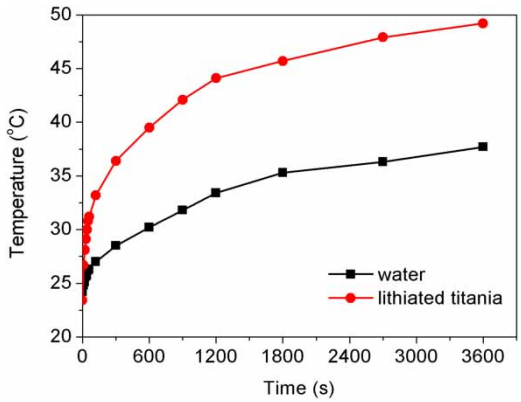

Figure 4 | The surface water temperatures versus time curves with and without lithiated titania.

10 minutes and then gradually increased to a maximum temperature of 49.2 °C within 60 minutes. The rapid temperature response was due to high absorbance in the entire solar spectrum of the lithiated titania (as shown in Figure 1(b)).

The effects of lithiated titania doses and solar light intensities on the water evaporation rate were studied to optimize the experimental conditions of the water evaporation. As shown in Figure 3(b), the optimized lithiated titania dose was 20 mg (or 6.2 $g{\cdot}m^{-2}$), and both a lower and larger lithiated titania dose led to a slightly decreased water evaporation rate. The former was because the water surface was not completely covered by the floating film, resulting in insufficient solar absorption. The latter was due to the overlapped floating film coverage, which hindered vapor transport velocity. As shown in Figure 3(c), the k values of lithiated titania floating film under 1, 2, and 5.5 sun solar light irradiance were 0.56, 0.87, and 2.63 $kg{\cdot}m^{-2}{\cdot}h^{-1}$ respectively, which were correspondingly 1.9, 2.4 and 4.2 times higher than that of the pure water. To test the stability and durability of the lithiated titania floating film, the water evaporation experiments were carried out after storage of the lithiated titania floating film in pure water for different periods including 1, 2, 3, 7, and 10 days. Almost no water

evaporation rate was lost over the whole measured period in pure water (Figure 3(d)), meaning a good stability and durability of the lithiated titania floating film.

Besides the water evaporation rate, the quality of the condensed fresh water should also be of concern. To evaluate the quality of the condensed fresh water, East China Sea water was used as source water for solar evaporation. The conductivity (salinity), turbidity, and TOC of the condensed fresh water dramatically reduced from 36,800 to 12 $\mu s \cdot cm^{-1}$, from 6.71 to 0.13 NTU, and from 6.7 to 3.4 $mg \cdot L^{-1}$ respectively. As shown in Figure 5(a)–5(c), these three water quality indicators were below the limit values defined by the World Health Organization (WHO) (World Health Organization 2011), the US Environmental Protection Agency (EPA) standards (US Environmental Protection Agency 2012) and the Standards for Drinking Water Quality in China (Chinese National Standards 2006). Moreover, the concentrations of cations (Na^+, K^+, Ca^{2+}, and Mg^{2+}) and anions (F^-, Cl^-, Br^-, NO_3^-, and SO_4^{2-}) in condensed fresh water also significantly decreased from 2.31–14,690 $mg \cdot L^{-1}$ to 0.08–0.94 $mg \cdot L^{-1}$ (see Figure 5(d)), which were far below the limit values defined by the above three water quality standards. Therefore, it was believed that the quality of the condensed fresh water, obtained by the lithiated titania floating film based on interfacial solar heating, satisfied the drinking water standards.

CONCLUSIONS

In summary, the synthesis process of hydrophobic lithiated titania and its formation of a thin floating film on the water surface, as well as its application in water evaporation based on interfacial solar heating, were demonstrated. The formation of a thin floating film significantly promoted water evaporation, which was due to the efficient use of the lithiated titania for solar light absorption and heat transfer. It is believed that the high water evaporation rate, excellent stability and durability, as well as the high quality of the condensed fresh water make the lithiated titania

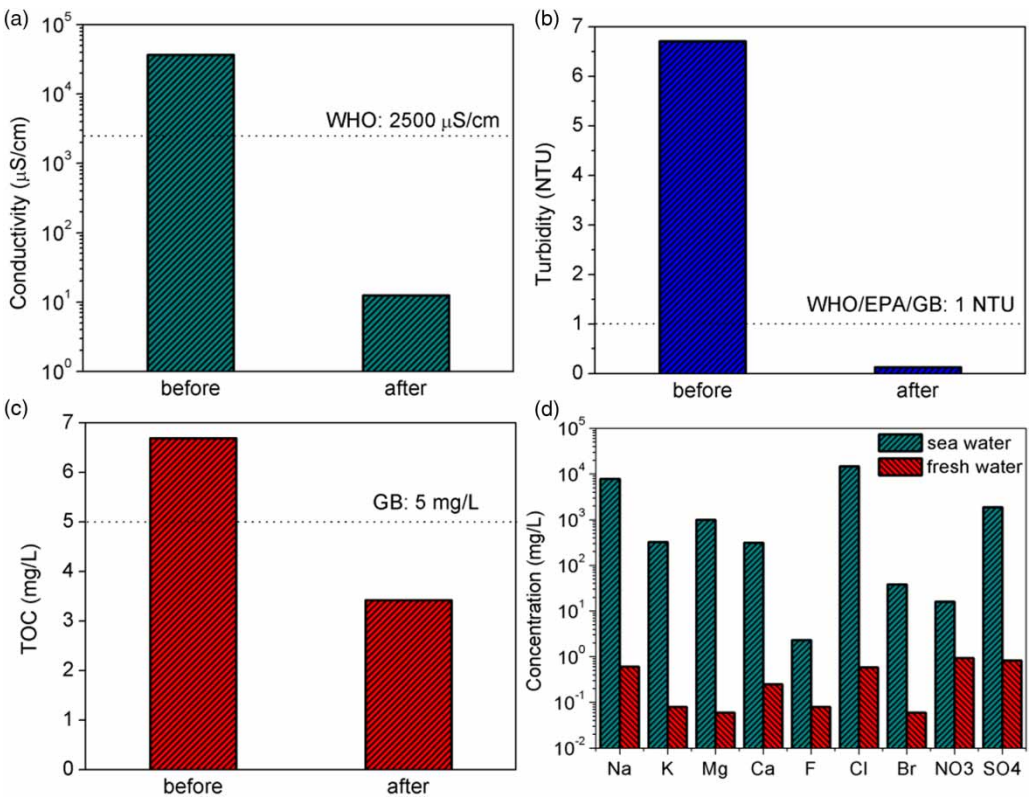

Figure 5 | The (a) conductivity, (b) turbidity, (c) total organic carbon (TOC) and (d) concentrations of typical cations and anions in seawater and condensed fresh water.

floating film potentially useful in solar desalination in some remote and rural areas.

ACKNOWLEDGEMENTS

The present work was financially supported by the National Science and Technology Major Protects for Water Pollution Control and Treatment (No. 2017ZX07201004), the Funds for International Cooperation and Exchange of the National Natural Science Foundation of China (No. 51761145022), the Public Welfare Technology Application Research Project of Zhejiang Province (No. LGG18E080002), and the Fundamental Research Funds for the Central Universities (No. 2018FZA4017).

SUPPLEMENTARY MATERIAL

The Supplementary Material for this paper is available online at https://dx.doi.org/10.2166/ws.2019.179.

REFERENCES

Chandrashekara, M. & Yadav, A. 2017 Water desalination system using solar heat: a review. *Renewable and Sustainable Energy Reviews* **67**, 1308–1330.

Chen, R., Wu, Z., Zhang, T., Yu, T. & Ye, M. 2017a Magnetically recyclable self-assembled thin films for highly efficient water evaporation by interfacial solar heating. *RSC Advances* **7** (32), 19849–19855.

Chen, R., Zhu, K., Gan, Q., Yu, Y., Zhang, T., Liu, X., Ye, M. & Yin, Y. 2017b Interfacial solar heating by self-assembled Fe_3O_4@C film for steam generation. *Materials Chemistry Frontiers* **1** (12), 2620–2626.

Chen, R., Wang, X., Gan, Q., Zhang, T., Zhu, K. & Ye, M. 2019 A bifunctional MoS_2-based solar evaporator for both efficient water evaporation and clean freshwater collection. *Journal of Materials Chemistry A* **7** (18), 11177–11185.

Chinese National Standards 2006 *Drinking Water Quality (GB 5749-2006)*. Available from: http://www.nhfpc.gov.cn/cmsresources/zwgkzt/wsbz/new/20070628143525.pdf.

Dao, V-D. & Choi, H.-S. 2018 Carbon-based sunlight absorbers in solar-driven steam generation devices. *Global Challenges* **2** (2), 1700094.

Ding, D., Huang, W., Song, C., Yan, M., Guo, C. & Liu, S. 2017 Non-stoichiometric MoO_{3-x} quantum dots as a light-harvesting material for interfacial water evaporation. *Chemical Communications* **53** (50), 6744–6747.

Gan, Q., Zhang, T., Chen, R., Wang, X. & Ye, M. 2019 Simple, low-dose, durable, and carbon-nanotube-based floating solar still for efficient desalination and purification. *ACS Sustainable Chemistry & Engineering* **7** (4), 3925–3932.

Hu, H., Wang, Z., Ye, Q., He, J., Nie, X., He, G., Song, C., Shang, W., Wu, J., Tao, P. & Deng, T. 2016 Substrateless welding of self-assembled silver nanowires at air/water interface. *ACS Applied Materials & Interfaces* **8** (31), 20483–20490.

Liu, Y., Chen, J., Guo, D., Cao, M. & Jiang, L. 2015 Floatable, self-cleaning, and carbon-black-based superhydrophobic gauze for the solar evaporation enhancement at the air–water interface. *ACS Applied Materials & Interfaces* **7** (24), 13645–13652.

Liu, Y., Wang, X. & Wu, H. 2017 High-performance wastewater treatment based on reusable functional photo-absorbers. *Chemical Engineering Journal* **309**, 787–794.

Shi, Y., Zhang, C., Li, R., Zhuo, S., Jin, Y., Shi, L., Hong, S., Chang, J., Ong, C. & Wang, P. 2018 Solar evaporator with controlled salt precipitation for zero liquid discharge desalination. *Environmental Science & Technology* **52** (20), 11822–11830.

Sing, K. S. W., Everett, D. H., Haul, R. A. W., Moscou, L., Pierotti, R. A., Rouquérol, J. & Siemieniewska, T. 1985 Reporting physisorption data for gas/solid systems with special reference to the determination of surface area and porosity (Recommendations 1984). *Pure and Applied Chemistry* **57** (4), 603–619.

Tao, P., Ni, G., Song, C., Shang, W., Wu, J., Zhu, J., Chen, G. & Deng, T. 2018 Solar-driven interfacial evaporation. *Nature Energy* **3** (12), 1031–1041.

US Environmental Protection Agency 2012 Edition of the Drinking Water Standards and Health Advisories, Office of Water. Available from: https://www.epa.gov/ground-water-and-drinking-water/table-regulated-drinking-water-contaminants.

Wang, Y., Zhang, L. & Wang, P. 2016 Self-floating carbon nanotube membrane on macroporous silica substrate for highly efficient solar-driven interfacial water evaporation. *ACS Sustainable Chemistry & Engineering* **4** (3), 1223–1230.

Wang, J., Li, Y., Deng, L., Wei, N., Weng, Y., Dong, S., Qi, D., Qiu, J., Chen, X. & Wu, T. 2017 High-performance photothermal conversion of narrow-bandgap Ti_2O_3 nanoparticles. *Advanced Materials* **29** (3), 1603730.

Wang, Y., Wang, C., Song, X., Huang, M., Megarajan, S. K., Shaukat, S. F. & Jiang, H. 2018 Improved light-harvesting and thermal management for efficient solar-driven water evaporation using 3D photothermal cones. *Journal of Materials Chemistry A* **6** (21), 9874–9881.

World Health Organization 2011 *Guidelines for Drinking-Water Quality*, 4th edn. World Health Organization, Geneva, Switzerland.

Xu, N., Hu, X., Xu, W., Li, X., Zhou, L., Zhu, S. & Zhu, J. 2017 Mushrooms as efficient solar steam-generation devices. *Advanced Materials* **29** (28), 1606762.

Ye, M., Zhang, Q., Hu, Y., Ge, J., Lu, Z., He, L., Chen, Z. & Yin, Y. 2010 Magnetically recoverable core–shell nanocomposites with enhanced photocatalytic activity. *Chemistry – A European Journal* **16** (21), 6243–6250.

Ye, M., Chen, Z., Zhang, T. & Shao, W. 2012 Effect of calcination temperature on the catalytic activity of nanosized TiO_2 for ozonation of trace 4-chloronitrobenzene. *Water Science and Technology* **66** (3), 479–486.

Zhou, L., Tan, Y., Wang, J., Xu, W., Yuan, Y., Cai, W., Zhu, S. & Zhu, J. 2016 3D self-assembly of aluminium nanoparticles for plasmon-enhanced solar desalination. *Nature Photonics* **10** (6), 393–398.

Zhu, L., Gao, M., Peh, C. K. N. & Ho, G. W. 2018a Solar-driven photothermal nanostructured materials designs and prerequisites for evaporation and catalysis applications. *Materials Horizons* **5** (3), 323–343.

Zhu, M., Li, Y., Chen, F., Zhu, X., Dai, J., Li, Y., Yang, Z., Yan, X., Song, J., Wang, Y., Hitz, E., Luo, W., Lu, M., Yang, B. & Hu, L. 2018b Plasmonic wood for high-efficiency solar steam generation. *Advanced Energy Materials* **8** (4), 1701028.

First received 24 June 2019; accepted in revised form 15 November 2019. Available online 5 December 2019